J Mater Sci (2007) 42:6177–6182
DOI 10.1007/s10853-006-1098-0

Mixed proton–electron conducting properties of Yb doped strontium cerate

Sun-Ju Song · Hyun-Soo Park

Received: 6 October 2005 / Accepted: 2 October 2006 / Published online: 17 April 2007

Abstract The electrical conductivity and hydrogen permeation properties of $SrCe_{0.8}Yb_{0.2}O_{3-d}$ membranes were studied as a function of temperature and P_{H_2} gradient. The bulk conductivity of $SrCe_{0.8}Yb_{0.2}O_{3-d}$ was an order of magnitude higher than the grain boundary conductivity over the temperature range 100–250 °C in feed gas of 4% H_2/balance He (pH_2O = 0.03 atm). The significantly lower grain boundary conductivity indicates that larger-grained materials might be more suitable for proton transport. The hydrogen flux through the membranes is proportional to thickness down to 0.7 mm. The hydrogen permeation flux increases with an increase in P_{H_2} gradient where the increase in hydrogen flux was explained by an increase in electron conduction as a function of temperature. The ambipolar conductivity calculated from hydrogen permeation fluxes shows the same P_{H_2} and P_{O_2} dependence as electron concentrations. The hydrogen and oxygen potential dependence of the ambipolar conductivity ($\log \sigma_{amb} = \log P_{H_2}^{1/2}$, $\log \sigma_{amb} = \log P_{O_2}^{1/4}$) was understood from the defect structure. From this, it was confirmed that hydrogen permeation might be limited by electron transport at wet reducing atmosphere. From the temperature dependence of the electronic conductivity, the activation energy calculated at wet reducing conditions is 0.63 eV.

S.-J. Song (✉) · H.-S. Park
Division of Materials Science and Engineering,
Chonnam National University, 300 Yongbong-dong,
Gwangju 500-757, Korea
e-mail: song@chonnam.ac.kr

Introduction

A growing attention in the development of an environmentally benign, inexpensive technology for separating hydrogen from water [1, 2] and/or syngas [3, 4] has motivated the research on proton conductors. Significant researches on proton conducting oxide have been performed over various chemical structures [5–8]. Among them, perovskite structure oxide is still preferably chosen as a prototype material for investigating its transport properties and defect structure due to the growing importance of this oxide for the use of hydrogen separation membranes, sensors, and fuel cells applications [9–12]. Especially, proton transport properties in multivalent cation-substituted strontium cerate have been studied over a number of years in this laboratory for hydrogen separation membrane application due to the high proton selectivity and the low oxygen ion conductivity of strontium cerate. Furthermore, the comparable ionic to electronic transference number is also required to be functional in non-galvanic mode. Ytterbium, in this study, was doped to strontium cerate due to its multivalent oxidation states, low ionization energy, and comparable ionic radius with cerium.

As is the case with other hydrogen separation membranes, the knowledge of defect structure and transport properties in this oxide will assist in understanding the nature of ambipolar diffusion of protons and electrons. A most common and straightforward way to measure the ambipolar diffusion properties may be via concentration cell measurements, but permeation measurement on mixed protonic–electroinc conductor oxides at elevated temperatures is normally subjected to experimental difficulties such as gas tight sealing problems. Therefore, extreme caution and know-how on permeation measurements are required

with establishing precise thermodynamic parameters for avoiding extraneous sources of error.

This paper begins by reporting the electrical and hydrogen permeation properties of SCYb. In this work, we report the both hydrogen flux and ambipolar conductivity of Yb-doped $SrCeO_{3-d}$ as a function of temperature, P_{O_2}, and P_{H_2} by hydrogen permeation measurements with well established experimental set-up.

Theory

Assuming a fixed Sr/(Ce+Me) ratio, the defect structure of multivalent cation doped strontium cerate may be well described by the external and internal equilibria. The defect structure of the $SrCe_{0.8}Yb_{0.2}O_{3-d}$ may also be understood on the basis of the irregular structure elements such as electron (e'), hole ($h^{\cdot}$), oxygen vacancies ($V_O^{\cdot\cdot}$), proton ($OH_O^{\cdot}$), cation vacancies (V''_{Sr}, V''''_{Ce}), and acceptor dopant (Yb'_{Ce} Yb''_{Ce}). The defect structure of the system will be described by relationships among structure elements. Mass action laws are applied to defect equilibria and Kroger–Vink notation is used [13].

(a) Internal equilibria

$$\text{null} = V''_{Sr} + V''''_{Ce} + 3V_O^{\cdot\cdot}; K_s = [V''_{Sr}][V''''_{Ce}][V_O^{\cdot\cdot}]^3 \quad (1)$$

where K_s is the equilibrium constant for Schottky–Wagner disorder.

$$\text{null} = e' + h^{\cdot}; K_i = n \cdot p \quad (2)$$

where K_i is the equilibrium constant for electron–hole pair intrinsic reaction.

(b) External equilibria

$$O_O^x = \frac{1}{2}O_2(g) + V_O^{\cdot\cdot} + 2e'; K_R = [V_O^{\cdot\cdot}]n^2P_{O_2}^{1/2} \quad (3)$$

where K_R is the equilibrium constant for exchange of oxygen.

$$H_2O(g) + V_O^{\cdot\cdot} + O_O{}^x = 2OH_O^{\cdot}; K_W = \frac{[OH_O^{\cdot}]^2}{[V_O^{\cdot\cdot}]P_{H_2O}} \quad (4)$$

where K_W is the equilibrium constant for exchange of water.

(c) Ionization equilibrium of doped Yb

$$Yb'_{Ce} = Yb''_{Ce} + h^{\cdot}; K_A = \frac{[Yb''_{Ce}]h^{\cdot}}{[Yb'_{Ce}]} \quad (5)$$

where K_A is the equilibrium constant for ytterbium ionization reaction.

(d) Overall external equilibria may be derived from Eqs. 3–5

$$\frac{1}{2}H_2O(g) + Yb'_{Ce} + O_O^x = OH_O^{\cdot} + Yb''_{Ce} + \frac{1}{2}O_2(g); K_O = \frac{[Yb''_{Ce}][OH_O^{\bullet}]P_{O_2}^{1/2}}{P_{H_2O}^{1/2}[Yb'_{Ce}]} \quad (6)$$

where K_o is the equilibrium constant for overall reaction.

(e) Charge neutrality condition

$$n + 2[Yb''_{Ce}] + [Yb'_{Ce}] = p + 2[V_O^{\cdot\cdot}] + [OH_O^{\cdot}] \quad (7)$$

The possibility of interstitial disorders is ruled out because they are energetically unfavourable in the perovskite structure from a structural viewpoint [14].

Once a hydrogen chemical potential gradient is applied, hydrogen will permeate due to the nature of ambipolar diffusion of proton and electrons determined by above defect equilibria. As the characteristics of hydrogen separation membranes severely count on the overall kinetics of the membrane oxides, overall kinetics of hydrogen permeation is a key information to optimizing the membrane devises. The overall hydrogen permeation process consists largely of three consecutive kinetic steps: gas/solid interfacial reaction, solid-state diffusion, and solid/gas interfacial reaction. For the $SrCe_{1-x}Yb_xO_{3-d}$ system, however, it has been reported in permeation studies at elevated temperature that the surface exchange reaction kinetics be fast enough, and overall kinetics is primarily governed by the solid-state diffusion step above 2 micrometer thick membrane [15]. By assuming bulk diffusion, the hydrogen permeation flux across an oxide membrane can be expressed by the Wagner equation [16]

$$J_{OH_O^{\cdot}} = -\frac{1}{L}\left\{\frac{RT}{4F^2}\int_{P'_{O_2}}^{P''_{O_2}}\sigma_t t_{OH_O^{\cdot}} t_{V_O^{\cdot\cdot}} d\ln P_{O_2} + \frac{RT}{2F^2}\int_{P'_{H_2}}^{P''_{H_2}}\sigma_t t_{OH_O^{\cdot}}(t_{V_O^{\cdot\cdot}} + t_{e'}) d\ln P_{H_2}\right\} \quad (8)$$

where σ_t is the total conductivity, t_i is the transference number of the charged species($I = OH_O^{\cdot}, V_O^{\cdot\cdot}, e'$), L is thickness of membrane, F is the Faraday constant and $d\ln P_{O_2}$ and $d\ln P_{H_2}$ are the chemical potential gradients across an oxide membrane.

Experimental

Polycrystalline $SrCe_{0.8}Yb_{0.2}O_{3-d}$ was prepared by conventional solid-state reaction methods. High-purity oxide powders of $SrCO_3$ (99.9% Alfa Aesar) and CeO_2 (99.9%

Alfa Aesar) were mixed with Yb_2O_3(99.99% Alfa Aesar) in a ball mill with stabilized zirconia media in isopropyl alcohol, and calcined at 1573 K for 10 h in air. The calcined oxides were then crushed, ground in a ball mill again for 24 h, pressed into pellets, and sintered at 1773 K for 10 h in air. Scanning electron micrograph of $SrCe_{0.8}Yb_{0.2}O_{3-d}$ is shown in Fig. 1. X-ray diffraction spectra confirmed a single phase with the orthorhombic perovskite structure as shown in Fig. 2.

The electrical conductivity was measured with an impedance analyzer (Solatron 1260). Pellets were coated with Pt paste (Engelhard 6929) and heated to 1273 K for 1 hr in air.

Hydrogen permeation was measured on dense disks (12 mm in diameter, 0.7, 0.9 and 1.4 mm thick). The planar surface of each disk were polished with 600 grit SiC polishing paper and then affixed to an alumina tube. A seal formed when the assembly was heated to 950 °C and the spring-loaded rods squeezed a gold ring between the membrane and the alumina tube. The sweep side flow was a constant 100 sccm of 100 ppm H_2/balanc N_2; the feed gas flow, 100 sccm of pure H_2 or 4% H_2/balance He. The flow rate of sweep gas during permeation measurements was controlled with a mass flow controller and was measured using a flow calibrator (Field_Cal 570 from Humonics). For the wet gas flow, feed gas mixture was bubbled through a water bath (EX-35D1 heating bath, Fisher Scientific) at room temperature. The hydrogen content of permeate stream was measured with Gas Chromatograph (HP 6890). Leakage of gas through pores in the sample or through an incomplete seal was checked by measuring the helium content of the permeate stream. The leakage rate obtained in this experiment was < 10 % of the total permeation flux.

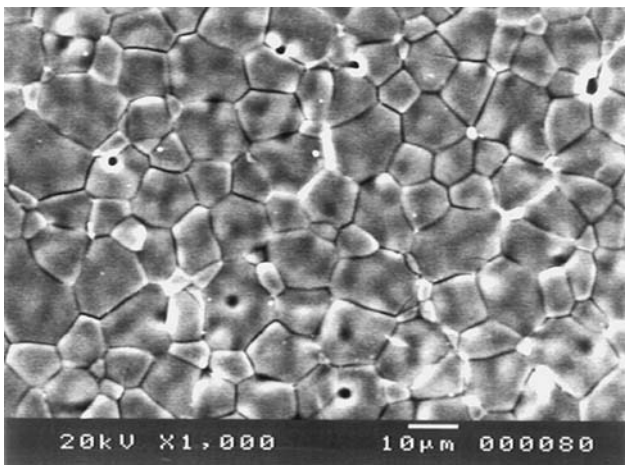

Fig. 1 SEM image of $SrCe_{0.8}Yb_{0.2}O_{3-\delta}$ membrane

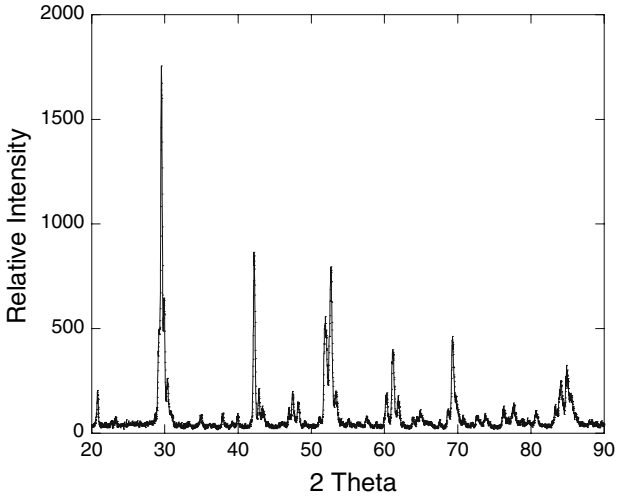

Fig. 2 X-ray diffraction pattern of $SrCe_{0.8}Yb_{0.2}O_{3-\delta}$ powders

Results and discussion

The electrical response of the SCYb samples below 250°C typically showed three semicircles in the impedance spectrum: one at high frequencies, corresponding to the bulk characteristics; one at medium frequencies, related to the grain boundary resistance, and one at low frequencies, associated with the electrode response. For calculating the grain and grain boundary resistivity from impedance measurements, we need the macroscopic and microscopic information about sample. Haile's group [17] reported the method of extracting resistivities by comparing the capacitance of the bulk and grain without further microscopic information while the bulk and grain boundary dielectric constants are approximately equal. A detailed mathematical explanation was given in [18]. Assuming an equivalent circuit of three parallel RC circuits connected in series, the impedance diagrams were fitted to obtain the resistance, characteristic frequency, and capacitance of the bulk, the grain boundary, and the electrodes. The Arrhenius plot of the electrical conductivity is shown in Fig. 3. The bulk conductivity was an order of magnitude higher than the grain boundary conductivity over the temperature range of 100–250 °C in a feed gas of 4% H_2/balance He (pH_2O = 0.03 atm), as shown in Fig. 3a. The calculated activation energy is 0.6 eV for bulk and grain boundary conduction. The significantly lower grain boundary conductivity indicates that larger-grained materials might be more suitable for proton transport. This finding suggests that the grain boundaries may not provide a pathway for fast proton transport, and that bulk transport makes a major contribution to the total conductivity at higher temperatures.

Above 600 °C, both the bulk and grain boundary response are incorporated into the high-frequency offset, leaving the electrode response as the only clearly defined

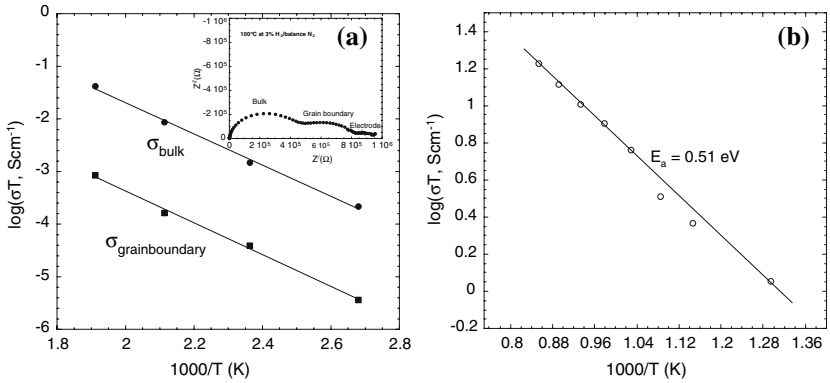

Fig. 3 Arrhenius plots of (**a**) bulk and grain boundary conductivity and (**b**) temperature dependence of total electrical conductivity of $SrCe_{0.8}Yb_{0.2}O_{3-\delta}$ at 4 % H_2/balance N_2 (pH_2O=0.03 atm)

semicircle. Figure 3(b) shows the Arrhenius plot of the temperature dependence of total conductivity of SCYb in 4% H_2 (pH_2O = 0.03 atm) feed gas at 500–900 °C. The calculated activation energy is 0.51 eV, which is a typical value for proton-conducting oxides.

From the hydrogen content measured in the sweep side of the permeation assembly and the sweep gas flow rate, the total hydrogen permeation rate was calculated assuming the ideal gas law. Then, the permeation flux was calculated by dividing the permeation rates by the surface area of the disk membranes.

Shown in Fig. 4 is the plot of hydrogen flux as a function of thickness at temperatures from 700 to 900 °C at wet 80 % H_2 conditions. The hydrogen flux through the membranes is proportional to thickness, indicating bulk diffusion kinetics is the rate limiting step in membranes investigated. The effect of increasing contribution from edge diffusion with increasing disk thickness may be significant but it is ruled out due to the good linear relationship from Fig. 4.

The influence of applied hydrogen chemical potential gradient at wet condition on the hydrogen permeability is shown in Fig. 5. The hydrogen permeation flux increases with an increase in P_{H_2} gradient. This trend is consistent with our previous results [19, 20] with Eu and Sm doped $SrCeO_{3-d}$.It was in our previous reports pointed out that electrons were still minor charge carriers in the wet reducing atmosphere, where protons were charge compensated by ionized dopant ions, and the electron transport in dopants was understood in terms of a charge transfer reaction between lower oxidation stated dopants to higher oxidation stated dopants [21]. The increase in hydrogen flux, therefore, may be explained by an increase in electron conduction as a function of temperature. In addition, the higher hydrogen flux compared with Eu and Sm doped system may also be interpreted in terms of ionization potential of each dopant because the ionized dopant

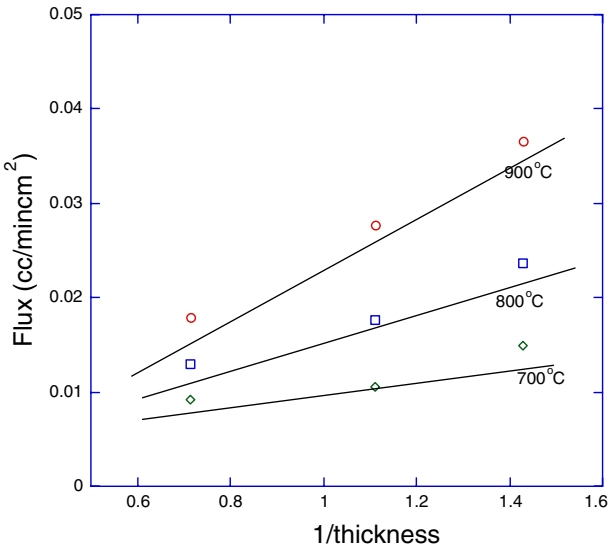

Fig. 4 Hydrogen flux as a function of thickness at wet 80% H_2 from 700 °C to 900 °C

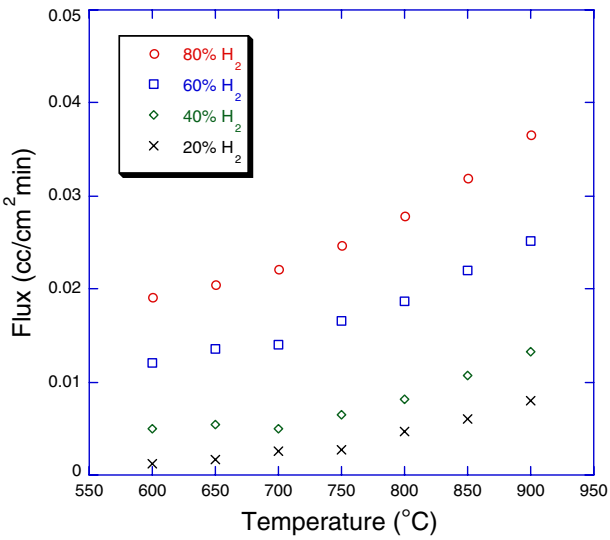

Fig. 5 Hydrogen flux as a function of temperature under various hydrogen chemical potential gradients

concentration depends on the ionization potential of each dopant under given thermodynamic conditions as reported previously. Therefore, the n-type electronic condition due to the $Yb''_{Yb} \rightarrow Yb'_{Yb} + e'$ is greater than the n-type conduction in Eu and Sm doped $SrCeO_{3-d}$.

Other factor that can influence electronic conductivity is polarizability because electron movement in the hopping mechanism is closely related with polarizability of dopant. The greater the difference in electronegativity between dopant cation and oxygen anion, the more polarizable the dopant is. Since the electronegativity of Yb is higher than Eu and Sm, the probability is greater that we will find hopping electrons polarized on the oxygen sites of the Eu, and Sm doped $SrCeO_{3-d}$ than Yb doped $SrCeO_{3-d}$. Therefore, the frequency of successful electron jumps between neighboring multivalent dopant ions decreases with an increasing difference in electronegativity to oxygen.

Because no discernible oxygen permeation during hydrogen permeation measurements was reported in $SrCeO_{3-d}$ membranes [19, 20], on the basis of Eq. 8, we can extract the ambipolar conductivity from the hydrogen flux.

$$\sigma_{amb} = \frac{\sigma_{OH_O^{\cdot}}\sigma_{e'}}{\sigma_{OH_O^{\cdot}} + \sigma_{e'}} = -\frac{4F^2L}{RT}\left\{\frac{\partial J_{H_2}}{\partial \log P''_{H_2}}\right\}_{P'_{H_2}} \tag{9}$$

where σ_i is the partial conductivity of the charged species ($I = OH_O^{\cdot}, e'$). F is the Faraday constant, L is membrane thickness and $\ln P''_{H_2}$ is the chemical potential at feed side of membrane. As shown in Fig. 6, the ambipolar conductivity varies with both P_{H_2} and P_{O_2}. Similar behaviour of the ambipolar conductivity was also reported on the system. The hydrogen and oxygen potential dependence of the ambipolar conductivity ($\log \sigma_{amb} = \log P_{H_2}^{1/2}$, $\log \sigma_{amb} = \log P_{O_2}^{1/4}$) may be well understood from the nature of defect structure of system [22]. In a wet reducing atmosphere with proton dominating regimes, the charge neutrality condition may be simplified to $[OH_O^{\cdot}] = 2[Yb''_{Ce}]$. With Eqs. 1–7, we may calculate the electron concentration as a function of thermodynamic parameters.

$$n = \left\{\frac{K_W K_R}{4[Yb]_t^2}\right\}^{1/2} P_{O_2}^{-1/4} P_{H_2O}^{1/2} \tag{10}$$

and by $K_{H_2O} = \frac{P_{H_2O}}{P_{O_2}^{1/2} P_{H_2}}$,

$$n = \left\{\frac{K_W K_R K_{H_2O}^2}{4[Yb]_t^2}\right\}^{1/2} P_{H_2}^{1/2} \tag{11}$$

where $[Yb]_t = [Yb'_{Ce}] + [Yb''_{Ce}]$. The hydrogen and oxygen potential dependence of the ambipolar conductivity is agreed with the dependence of electron concentration within the regimes investigated. As the ambipolar conductivity shows the same P_{H_2} and P_{O_2} dependence as electron concentrations, hydrogen permeation may be limited by electron transport. Therefore, the ambipolar conductivity can be considered equivalent to the electron conductivity in this experiments, where protons are charge compensated by ionized ytterbium ions.

If we assume that $\sigma_{amb} \approx \sigma_{e'}$, the electronic conductivity as a function of temperature at 80% H_2 is as shown in Fig. 7. From the temperature dependence of the electronic conductivity, the activation energy calculated at wet reducing conditions is 0.63 eV, which is somewhat lower than that of Eu doped $SrCeO_{3-d}$ (0.72 eV) [19].

Conclusions

The bulk conductivity of $SrCe_{0.8}Yb_{0.2}O_{3-d}$ was an order of magnitude higher than the grain boundary conductivity over the temperature range 100–250 °C in feed gas of 4% H_2/balance He (pH_2O = 0.03 atm). The significantly lower grain boundary conductivity indicates that larger-grained materials might be more suitable for proton transport.

Hydrogen permeability of $SrCe_{0.8}Yb_{0.2}O_{3-d}$ membranes was studied by measuring gas permeation as a function of temperature and P_{H_2} gradient. The hydrogen flux through the membranes is proportional to thickness down to 0.7 mm, indicating that bulk diffusion kinetics is the rate limiting step

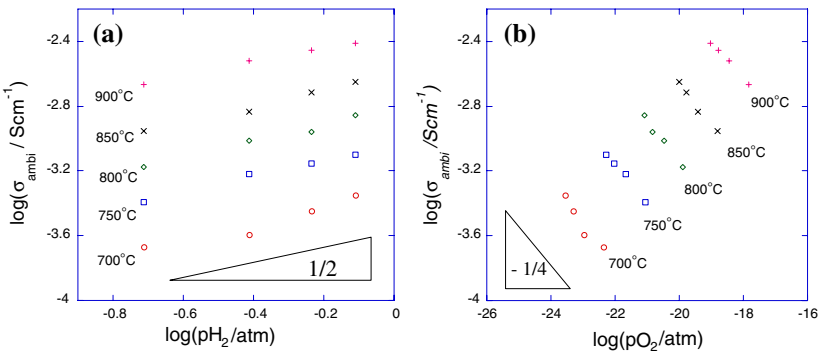

Fig. 6 Ambipolar conductivity as a function of (**a**) pH_2, (**b**) pO_2

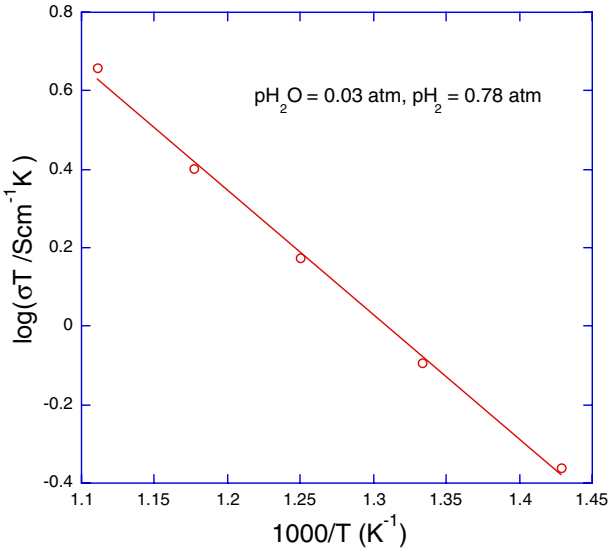

Fig. 7 Electronic conductivity as a function of temperature

in membranes investigated. The hydrogen permeation flux increases with an increase in P_{H_2} gradient where the increase in hydrogen flux was explained by an increase in electron conduction as a function of temperature.

The ambipolar conductivity calculated from hydrogen permeation fluxes shows the same P_{H_2} and P_{O_2} dependence as electron concentrations. The hydrogen and oxygen potential dependence of the ambipolar conductivity ($\log \sigma_{amb} = \log P_{H_2}^{1/2}$, $\log \sigma_{amb} = \log P_{O_2}^{1/4}$) was understood from the defect structure of system while the charge neutrality condition may be simplified to $[OH_O^{\cdot}] = 2[Yb_{Ce}'']$. From this, it was confirmed that hydrogen permeation might be limited by electron transport at wet reducing atmosphere. From the temperature dependence of the electronic conductivity, the activation energy calculated at wet reducing conditions is 0.63 eV.

References

1. Balachandran U, Lee TH, Wang S, Dorris SE (2004) Inter J Hydrogen Energy 29:291
2. Song S-J, Wachsman ED (2006) Chem Lett 35:1068
3. Siriwardane RV, Poster JA, Fisher EP, Lee TH, Dorris SE, Balachandran U (2000) App Surf Sci 167:34
4. Balachandran U, Mar B, Maiya PS, Mieville RL, Dusek JT, Picciole J, Guan J, Dorris SE, Liu M (1998) Solid State Ionics 108:363
5. Du Y, Nowick S (1995) J Amer Ceram Soc 78:3033
6. Kreuer KD (1999) Solid State Ionics 125:285
7. Song S-J, Wachsman ED, Dorris SE, Balachandran U (2002) Solid State Ionics 149:1
8. Poulsen FW (1999) J Solid State Chem 143:115
9. Balachandran U, Lee TH, Wang S, Picciolo J, Dusek JT, Dorris SE (2000) Amer Chem Soc, 224:169-fuel part 1, Aug. 18,
10. Iwahara H (1995) Solid State Ionics 77:289
11. Iwahara H (271) Solid State Ionics 125:271
12. Haile SM, Boysen DA, Chisholm CRL, Merle RB (2002) Nature 410:910
13. Kroger FA, Vink VJ (1956) In: Seitz F, Turnbull D (eds) Relations between the concentrations of imperfections in crystalline solids solid state physics, vol 3. Academic Press, New York, pp 307–405
14. Lewis GV, Catlow CRA (1983) Radiat Eff 73:307
15. Hamakawa S, Anwa L, Iglesia E (2002) Solid State Ionics 148:71
16. Song S-J, Wachsman ED, Rhodes J, Dorris SE, Balachandran U (2003) Solid State Ionics 164:107
17. Haile SM, West DL, Campbell J (1998) J Mater Res 13:1576
18. Macdonald JR (1987) Impedance spectroscopy. J. Wiley & Sons, New York
19. Song S-J, Wachsman ED, Rhodes J, Dorris SE, Balachandran U (2004) Solid State Ionics 167:99
20. Song S-J, Wachsman ED, Rhodes J, Yoon H-S, Zhang G, Lee K-H, Dorris SE, Balachandran U (2005) J Mater Sci 40:4061
21. Song S-J, Wachsman ED, Dorris SE, Balachandran U (2003) J Electrochem Soc 150:A790
22. Song S-J, Wachsman ED, Dorris SE, Balachandran U (2003) J Electrochem Soc 150:A1484